Mechanistic Understanding Enables Chemoselective sp^3 over sp^2 C-H Activation in Pd-Catalyzed Carbonylative Cyclization of Amino Acids

SCHOLARONE™
Manuscripts

ARTICLE

Mechanistic Understanding Enables Chemoselective sp³ over sp² C–H Activation in Pd-Catalyzed Carbonylative Cyclization of Amino Acids

Mario Martínez-Mingo,[a] Inés Alonso,*[a,b] Nuria Rodríguez,*[a,b] Ramón Gómez Arrayás*[a,b] and Juan C. Carretero[a,b]

Mechanistic insights into the factors that control chemoselectivity in competing C(sp²)–H and C(sp³)–H activation pathways in the palladium-catalyzed carbonylative cyclization of γ-arylated valine type derivatives, gained by experimental observations and DFT studies, have been leveraged to reverse the remarkable selectivity of Pd for arene C(sp²)–H activation over C(sp³)–H cleavage. These studies suggest that ε-C(sp²)–H bond cleavage is significantly faster and more reversible than the γ-C(sp³)–H bond activation, whereas subsequent AcOH/CO exchange and CO insertion from the C(sp³)-palladacycle lead to more stable intermediates from which the reaction is irreversible. Control of chemoselectivity has been achieved by playing on the reaction conditions to favour thermodynamic over kinetic control. Addressing this fundamental limitation of C–H functionalization under Pd-catalysis has enabled the access to different heterocyclic frameworks (i.e., γ-lactams instead of benzazepinone skeletons) from the same starting substrate.

Introduction

Recent advances on controlling regioselectivity and functional group tolerance in catalytic direct C–H functionalization have made possible elegant applications to complex molecule synthesis and late-stage diversification of existing compounds to rapidly improve their properties.[1,2] However, despite this spectacular progress, control of chemoselectivity in molecules possessing different types of C–H bonds that can potentially undergo activation remains as a big challenge.[1] Chelation-assisted cyclometallation has traditionally been the primary strategy to ensure the desired selectivity,[3] favoring the selective formation of one specific product. In contrast, strategies capable of overriding the innate relative reactivity of distinct reactive C–H bonds by careful choice of catalysts/conditions are still quite difficult and rare,[4,5] yet highly attractive since they enable the access to diverse scaffolds. In particular, achieving selective functionalization of specific 'inert' sp³ C–H bonds in molecules containing accessible, and intrinsically more reactive, sp² C–H bonds remains as a fundamental limitation. Although there are available a number of catalyst systems capable of achieving divergent site-selectivity in molecules where more than one type of C(sp²)–H bond can potentially undergo reaction,[4] the ability to program chemoselective activation of

C(sp³)–H over C(sp²)–H bonds has been rarely documented.[5,6] Most of the latter applications involve the directed activation of benzylic methyl C–H bonds.[5a-g]

Recently, directed Pd-catalyzed C(sp³)–H functionalization exploiting favored 5-membered ring cyclopalladation pathway has been extensively explored, especially in amino acid derivatization chemistry.[7] In this context, we reported a Pd-catalyzed carbonylative cyclization of aliphatic amines and amino acids via γ-C(sp³)–H activation, leading to γ-lactam derivatives.[8] During our structure scope analysis, we discovered that substrates having an aryl group, such as γ-aryl-substituted L-valine derivatives (**1**), showed a preference to undergo more remote ε-C(sp²)–H bond cleavage to form benzazepinone derivatives (**2**, Scheme 1, left).[9]
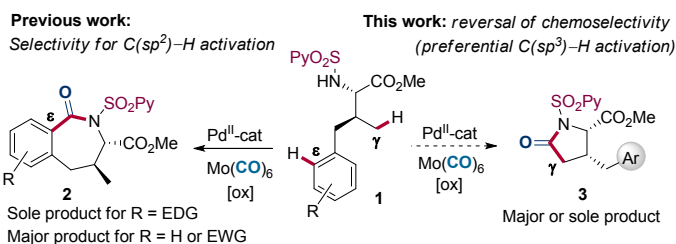
Scheme 1. Reversal of sp²/sp³ C–H activation chemoselectivity in Pd-catalyzed carbonylative cyclization of amines.

Our investigations revealed that although remote aromatic C(sp²)–H over aliphatic γ-C(sp³)–H activation was consistently preferred, the electronic properties of the aromatic ring showed a remarkable influence on chemoselectivity. Thus, substituents with electron-donating character resulted in excellent chemoselectivity towards the C(sp²)–H activation

[a.] Department of Organic Chemistry, Universidad Autónoma de Madrid, c/ Fco. Tomás y Valiente 7, Cantoblanco 28049, Madrid (Spain).
[b.] Institute for Advanced Research in Chemical Sciences (IAdChem), Universidad Autónoma de Madrid (UAM).
† Footnotes relating to the title and/or authors should appear here.
Electronic Supplementary Information (ESI) available: [details of any supplementary information available should be included here]. See DOI: 10.1039/x0xx00000x

product, whereas ones with electron neutral or electron withdrawing demand displayed lower selectivity (Scheme 1, left). Nevertheless, this unusual 7-membered ring cyclopalladation mode, which predominated even when more common 5-membered γ-C(sp^3)–H cyclopalladation pathways are accessible, showcases the remarkable selectivity for arene C–H activation over aliphatic C–H activation displayed by Pd.[10] We hypothesized that a theoretical and experimental investigation of the reaction mechanism and the factors that govern site-selectivity of competing C–H functionalization pathways, could provide insight that will enable reversing the sp^2 over sp^3 chemoselectivity in Pd-catalyzed C–H activation towards the access of γ-lactams **3** (Scheme 1, right). As an advance toward this goal, herein we describe the reversal of the conventionally preferred C(sp^2)–H activation to favor C(sp^3)–H activation in Pd-catalyzed carbonylative cyclization of amino acid derivatives. Control of chemoselectivity was achieved by playing on the reaction conditions to achieve either thermodynamic or kinetic control upon a solid understanding on the mechanism and the factors controlling selectivity.

Results and discussion

**Computational studies.** We initiated our studies digging into the factors favoring the formation of benzazepinone (through ε-C(sp^2)–H bond activation) over the γ-lactam (via γ-C(sp^3)–H cleavage) product in the Pd-catalyzed carbonylative cyclization of the γ-phenyl-L-valine derivative **1a** (R = H) in dioxane.

We studied the coordination mode of **1a** to the Pd center (Figure 1). The most stable species of Pd-acetate is the trimeric complex Pd$_3$(OAc)$_6$, in which each of the three Pd atoms is in a square-planar environment.[11,12] Its endergonic dissociation to dimeric or monomeric Pd-acetate species, as well as its favorable transformation into monomeric salts of other anions (starting material, etc.) has been computationally studied.[13] Based on our own experimental data,[14] we considered that such dissociation might be coupled with a metatheses process with two units of **1a** to form acetic acid and the stable monomeric **IM1-1a** as a viable intermediate. Since an analogous complex had proved to be a competent catalyst precursor[9] and similar Pd salts had been proposed to evolve, directly or through the participation of bimetallic complexes with Ag,[13d] into the corresponding C–H activation products, we first studied the C–H activation step from intermediate **IM1-1a**. However, the activation barriers found were quite high (see SI information for details) and thus, we decided to study the process from the simpler intermediate **IM2-1a**, easily formed from **IM1-1a** through coordination of an acetic acid molecule to the Pd center and displacement of **1a**.[15] This endergonic step bears a considerable activation energy barrier of 18.1 kcal·mol^{-1} since it entails the loss of coordination of Pd atom to the Py unit and all the stabilizing π-stacking interactions existing in **IM1-1a**. The resulting intermediate **IM2-1a** is less stable than **IM1-1a** because the metal is located in a distorted square-planar arrangement (compare angles N-Pd-N ≈ 86° _vs_. O-Pd-O: 63°). However, this complex shows a remarkable stabilizing interaction between the carbonylic oxygen lone pairs of the

ester group and the Pd atom (Pd–O distance is 3.142 Å, close to the sum of their van der Waals radii) that is also observed in subsequent intermediates and might play an important role in the observed selectivity (_vide infra_).

IM2-1a is the common intermediate for **<u>Path A:</u>** The ε-C(sp^2)–H bond activation to form the benzazepinone **2a** (R = H), and **<u>Path B:</u>** The γ-C(sp^3)–H bond cleavage to form the γ-lactam **3a** (Ar = Ph), as shown in Figure 2
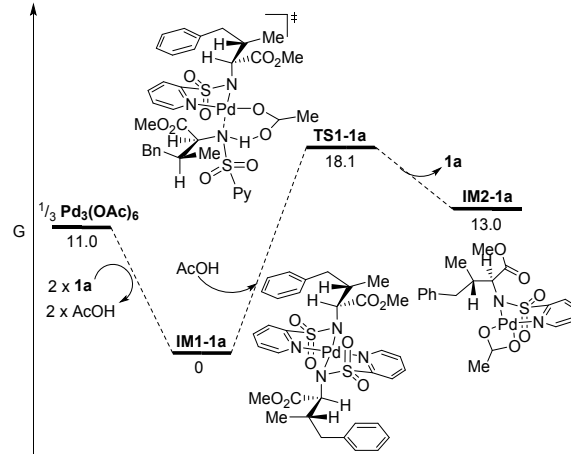

Figure 1. Energy profile for the coordination of AcOH to the Pd center and the formation of complex **IM2-1a** in 1,4-dioxane (M06$_{SMD}$ / 6-311++G(d,p) (C,H,N,O,S), SDD (Pd) // B3LYP-D3 / 6-31G(d) (C,H,N,O,S), LANL2DZ(f) (Pd). Relative G values at 298 K (kcal·mol^{-1}).

ε-C(sp^2)–H bond activation (path A) (in black): **TS2-A-1a** was found to be the most stable transition state (27.1 kcal·mol^{-1}) from intermediate **IM2-1a**.[16] The seven-membered cycle formed by Pd, N and the rest of the amino acid moiety, adopts a distorted boat-like conformation, with Pd atom and β-C located on the peaks of the boat and the ε-C–Pd bond almost completely formed (2.108 Å). The C–H bond undergoing cleavage lies out of the plane δ-C–ε-C–Pd–N, with the H atom closer to the acetate group (distances C–H and H–O are 1.405 and 1.259 Å respectively), which differs from conventional concerted metalation-deprotonation (CMD) mechanism. In this regard, although an electrophilic palladation has been proposed in the functionalization of remote aryl C–H bonds,[17] a Wheland-type intermediate could not be found.

The C–H activation process leads to a bicyclic seven-five-membered palladacycle intermediate **IM3-A-1a** (17.7 kcal·mol^{-1}), which then readily drops to intermediate **IM4-A-1a** by displacement of acetic acid in the presence of CO. Intermediate **IM4-A-1a** is a palladium(II) complex stabilized by the pyridine ring and the CO molecule (3.8 kcal·mol^{-1}). However, such stabilization could be compromised if another molecule of CO coordinates, displacing the pyridine N from the coordination plane to give **IM5-A-1a** (7.2 kcal·mol^{-1}).[18] For intermediate **IM5-A-1a**, carbonyl insertion requires an energy barrier of 12.2 kcal·mol^{-1}, reaching **TS3-A-1a** where the Pd–C$_ε$ bond is being cleaved while the C$_ε$–CO bond is being formed in a concerted way via a three membered-ring. The eight-five-membered palladium(II) intermediate **IM6-A-1a** is thus obtained, in which the other vacancies are occupied by a CO ligand and the pyridine ring (−6.4 kcal·mol^{-1}). The reductive

elimination, proceeds via a transition state in which the N–CO bond is being formed while the Pd–CO bond is being cleaved [**TS4-A-1a** (6.0 kcal·mol^{-1})], leading to the bicyclic intermediate **IM7-A-1a** (−21.0 kcal·mol^{-1}). This intermediate shows a quite folded structure, that locates the ester moiety in parallel arrangement to the aromatic ring, allowing a higher degree of conjugation between the latter and the carbonyl group than in previous intermediates, hence increasing its stability. Subsequently, to close the catalytic cycle, **IM7-A-1a** undergoes product dissociation of Pd(0), followed by oxidation of the metal to regenerate the Pd(II) catalyst by the combined action of a Ag(I) salt and benzoquinone. This process is expected to be highly exergonic with low activation barriers. The details of these steps were not calculated.

It should be noted that the C–H bond cleavage is the step with the highest-energy transition state but the formation of intermediate **IM2-1a** is presumably the step with the highest activation barrier (18.1 kcal·mol^{-1}).

γ-C(sp^3)–H bond activation (path B) (in blue): Based on our previous studies,[8] the γ-C(sp^3)–H activation may occur through a CDM pathway starting from intermediate **IM2-1a**. This step was found to take place through **TS2-B-1a** (33.8 kcal·mol^{-1}), in which the six-membered cycle formed by Pd, amine N and the rest of the amino acid moiety, including the C–H bond being cleaved, adopts a distorted chair-like conformation, with the ester and benzyl groups located in axial and equatorial positions

respectively. The γ-C–Pd, C–H and H–O distances (2.220, 1.414 and 1.333 Å respectively) are in agreement with those found in previous studies.[8] The resulting intermediate **IM3-B-1a** easily evolves through ligand exchange between the acetic acid and CO, generating the highly stable complex **IM4-B-1a** (−1.2 kcal·mol^{-1}), from which the reaction is irreversible.

The migratory insertion of CO into the Pd–C bond seems to be facilitated by previous coordination of a second molecule of CO[18] along with a change in the conformation of the palladacycle [**IM5-B-1a** (−0.9 kcal·mol^{-1})]. From this intermediate, the most stable transition state found was **TS3-B-1a** (22.6 kcal·mol^{-1}) with the ester and benzyl groups located in equatorial and axial positions, respectively. Once this high barrier is overcome, **TS3-B-1a** eagerly leads to the stable intermediate **IM6-B-1a** (−12.8 kcal·mol^{-1}). Complex **IM6-B-1a** might evolve through the reductive elimination transition state **TS4-B-1a**, where the N–CO bond is being formed as the Pd–CO bond is being cleaved (−3.5 kcal·mol^{-1}), to generate the cyclic intermediate **IM7-B-1a** (−23.9 kcal·mol^{-1}). In this complex, the ester and benzyl moieties keep their pseudoequatorial and axial arrangement respectively in the five-membered cycle.

Analysis of this energy profile, reveals that the C–H bond cleavage is also here the step with highest-energy transition state but the migratory insertion of CO into the Pd–C bond is the step with the highest activation barrier (23.5 kcal·mol^{-1}).
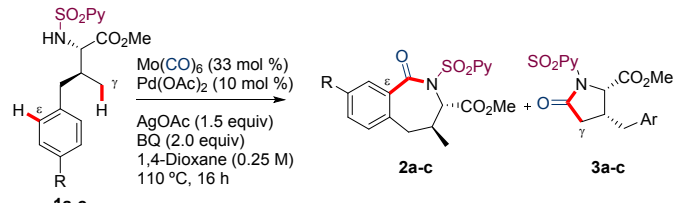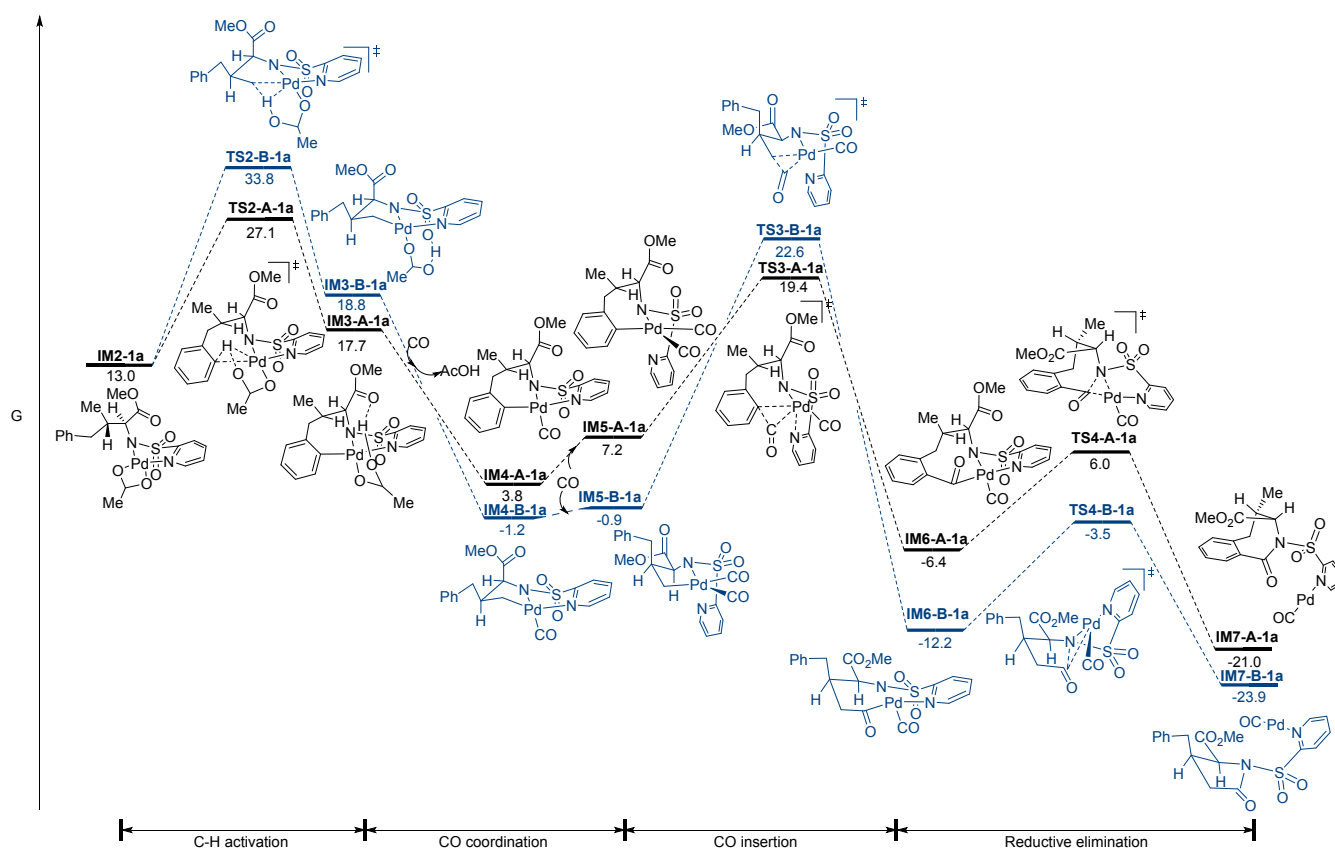

Figure 2. Energy profile for the Pd(II) catalyzed transformation of substrate **1a** into γ-lactam and benzazepinone complexes in 1,4-dioxane (M06$_{SMD}$ / 6-311++G(d,p) (C,H,N,O,S), SDD (Pd) // B3LYP-D3 / 6-31G(d) (C,H,N,O,S), LANL2DZ(f) (Pd)). Relative G values at 298 K (kcal·mol^{-1}).

Origins of chemoselectivity. As mentioned in the introduction, the Pd-catalyzed carbonylative cyclization of the γ-phenyl-L-valine derivative **1a** (R = H) in dioxane favours the formation of the benzazepinone **2a** over the formation of the γ-lactam **3a**, albeit the selectivity is low. However, the relative ratio of products experimentally observed cannot be easily rationalized on the basis of one 'determining step or state' in the catalytic cycle. By comparing both reaction pathways (Figure 2), one could draw two conclusions: i) the C–H bond cleavage should be faster in ε-C(sp^2) than in γ-C(sp^3) [**TS2-A-1a** (27.1 kcal·mol^{-1}), **TS2-B-1a** (33.8 kcal·mol^{-1})], and ii) the benzazepinone complex **IM7-A-1a** is relatively less stable than the γ-lactam complex **IM7-B-1a** (−21.0 and −23.9 kcal·mol^{-1}, respectively). Therefore, the benzazepinone **2a** would correspond to a product obtained under kinetic control conditions whereas the γ-lactam **3a** would be the thermodynamic control product of the process. Nonetheless, the correlation between DFT calculations and experimental data is more complex. The ε-C(sp^2)–H bond cleavage is significantly faster but more reversible than the γ-C(sp^3)–H bond activation. Therefore, the reverse ε-C(sp^2)–H bond cleavage leads back to **IM2-1a** and the reaction can now evolve through γ-C(sp^3)–H bond activation and irreversible CO insertion, followed by reductive elimination to yield product-coordinated complex **IM7-B-1a**.

Influence of the substituents of the aromatic ring on the selectivity. As alluded to in the introduction, in our previous studies on *N*-SO$_2$Py-assisted Pd-catalyzed carbonylative cyclization of γ-aryl-L-valine derivatives **1**, we had observed that electronic effects strongly influenced both reactivity and chemoselectivity.[9] Representative results shown in Table 1 illustrate that the reactivity decreases on lowering the electron density of the aromatic ring. In addition, whereas the carbonylative cyclization of substrates bearing electron-rich aryl groups provided the corresponding benzazepinone products with complete ε-C(sp^2)–H selectivity (entry 2), those with

electron-neutral or, electron-deficient aryls were significantly less selective (entries 1 and 3).

Table 1. Influence of electronic effects of the aryl group on chemoselectivity.

Entry[a]	R (substrate)	2, (%)[b]	3 (%)[b]
1	H (**1a**)	**2a**, 57	**3a**, 27
2	Me (**1b**)	**2b**, 80	**3b**, –
3	CF$_3$ (**1c**)	**2c**, 22	**3c**, 21

[a] Reaction conditions: **1** (0.10 mmol), Mo(CO)$_6$ (0.033 mmol, 30 mol %), Pd(OAc)$_2$ (0.01 mmol, 10 mol %), AgOAc (0.15 mmol, 1.5 equiv), 1,4-benzoquinone (BQ) (0.20 mmol, 2.0 equiv), 1,4-dioxane (0.40 mL), 110 °C, 16 h, under argon atmosphere. [b] Isolated yields.

To gain an insight into the influence that the electronic character of the substituents might exert on the reactivity and selectivity of the process, key transition states and intermediates were analysed for the functionalization of the γ-*p*-tolyl-L-valine derivative **1b** (R = 4-Me) and the γ-trifluoromethylphenyl-L-valine substrate **1c** (R = 4-CF$_3$). Table 2 summarizes the most relevant data. This comparison revealed that the electronic character of the aryl ring plays a significant role in controlling the energy barrier for initial ligand displacement by AcOH upon coordination of **1** to the palladium center (from **IM1** to **IM2**). The lower reactivity of CF$_3$-substituted substrate **1c** may be attributed to the higher activation barrier to reach **TS1** (20.6 kcal·mol^{-1}) compared to that for **1a** (18.1 kcal·mol^{-1}) or **1b** (17.6 kcal·mol^{-1}). The aryl substituent, however, seems to have no significant influence in the stability of intermediate **IM2**.

Table 2. Comparison of the key steps for the competitive synthesis of benzazepinone versus γ-lactam from **1a**, **1b** and **1c** in 1,4-dioxane (M06SMD / 6-311++G(d,p) (C,H,N,O,S,F), SDD (Pd) // B3LYP-D3 / 6-31G(d) (C,H,N,O,S,F), LANL2DZ(f) (Pd). Relative G values at 298 K (kcal·mol^{-1}).

Ar	IM1 dissociation			C–H activation				CO coordination		CO insertion	
	IM1	TS1	IM2	TS2-A	TS2-B	IM3-A	IM3-B	IM4-A	IM4-B	TS3-A	TS3-B
C$_6$H$_5$ (**1a**)	0	18.1	13.0	27.1	33.8	17.7	18.8	3.8	-1.2	19.4	22.6
p-Me-C$_6$H$_4$ (**1b**)	0	17.6	12.3	26.3	32.7	16.3	17.8	2.5	-2.1	18.1	21.6
p-CF$_3$-C$_6$H$_4$ (**1c**)	0	20.6	12.7	28.6	35.0	18.9	18.9	4.6	-0.1	21.9	25.3

To understand the reasons behind this difference in reactivity, we looked into the optimal geometries for **IM1-1a**, **IM1-1b** and **IM1-1c** (Figure 3). The electronic character of the substituent seems to be related to the slight variation of certain geometric parameters that could explain the different barriers. To reach the corresponding **TS1**, AcOH has to displace pyridinic N2 from palladium whose bond with the metal is weakened when R =

Me (centroid distance r^1-r^2 shows the smaller value) but slightly strengthened with the CF$_3$ group. At the same time, this electronic effect between rings causes a conformational change in the amino acid moiety (compare torsion angles) that might hinders the approach of AcOH during ligand exchange in the order **1c>1a>1b**.
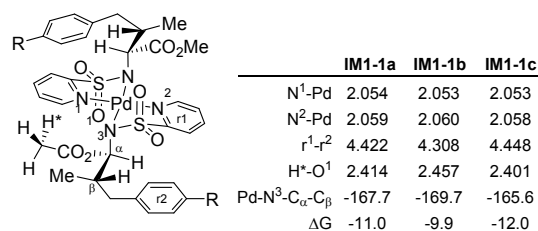
Figure 3. Comparison of optimal geometries for **IM1-1a**, **IM1-1b** and **IM1-1c**. Relevant distances (Å) and a torsion angle (°) are indicated. ΔG (kcal·mol⁻¹) relative to Pd₃(OAc)₆ in 1,4-dioxane.

	IM1-1a	IM1-1b	IM1-1c
N^1-Pd	2.054	2.053	2.053
N^2-Pd	2.059	2.060	2.058
r^1-r^2	4.422	4.308	4.448
H^*-O^1	2.414	2.457	2.401
Pd-N^3-C_α-C_β	-167.7	-169.7	-165.6
ΔG	-11.0	-9.9	-12.0

To rationalize how the $C(sp^2)$–H/$C(sp^3)$–H chemoselectivity is influenced by the electronic character of the aryl substituents, we focused on the subsequent steps throughout the catalytic cycle. In the ε-$C(sp^2)$–H bond cleavage step from **IM2**, it was found that the lower the electron density of the aromatic ring, the higher the energy of **TS2-A** (Table 2, 27.1 kcal·mol⁻¹ for **TS2-A-1a**, 26.3 kcal·mol⁻¹ for **TS2-A-1b** and 28.6 kcal·mol⁻¹ for **TS2-A-1c**).

Interestingly, the same trend was observed for the relative stability of intermediate **IM3-A** (17.7 kcal·mol⁻¹ for **IM3-A-1a**, 16.3 kcal·mol⁻¹ for **IM3-A-1b** and 18.9 kcal·mol⁻¹ for **IM3-A-1c**). These data suggest that the lower the electron density of the ring, the more reversible is the ε-$C(sp^2)$–H bond cleavage (**IM3-A** is less stable than **IM2**: 4.7, 4.0 and 6.2 kcal mol⁻¹ for **1a**, **1b** and **1c** respectively). This effect is consistent with the lower selectivity experimentally observed in the ε-$C(sp^2)$–H carbonylation of the CF₃-substituted substrate **1c** (Table 1). In this context, a regime for reversible $C(sp^2)$–H would be favoured and, then, evolution of **IM2** through γ-$C(sp^3)$–H cleavage/irreversible CO insertion towards the thermodynamically more stable γ-lactam derivative can become a competitive pathway.

A careful analysis of the structure of intermediates **IM3-A** revealed small differences that could explain the lower stability caused by the presence of electron-withdrawing groups. In particular, the natural atomic charge at the reactive C_ε becomes positive for the **IM3-A** complex derived from **1c** (**IM3-A-1c**), in contrast to the slightly negative values of charge found at C_ε in related complexes derived from **1a** and **1b** (Figure 4). This effect seems to be counterbalanced by strengthening the electron donation from the lone pairs of ester carbonyl oxygen (O^1) to Pd atom, as evidenced by the decreased value of the calculated O^1–Pd distance. However, this increased stabilizing interaction comes at the cost of a slight conformational change of the seven-membered cycle that increases the torsional strain of several bonds, specially that between N and C_γ.
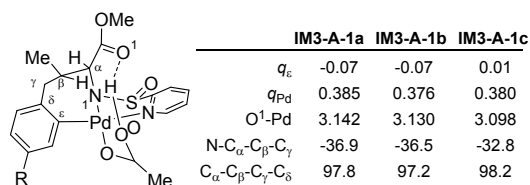

Figure 4. Comparison of optimal geometries for **IM3-A-1a**, **IM3-A-1b** and **IM3-A-1c**. Relevant natural charges (a.u.), distance (Å) and torsion angles (°) are indicated.

	IM3-A-1a	IM3-A-1b	IM3-A-1c
q_ε	-0.07	-0.07	0.01
q_{Pd}	0.385	0.376	0.380
O^1-Pd	3.142	3.130	3.098
N-C_α-C_β-C_γ	-36.9	-36.5	-32.8
C_α-C_β-C_γ-C_δ	97.8	97.2	98.2

The data shown in Table 2 show that the same trend extends to the γ-$C(sp^3)$–H bond cleavage: the lower the electron density of the aromatic ring, the higher the energy of **TS2-B** (33.8 kcal·mol⁻¹ for **TS2-B-1a**, 32.7 kcal·mol⁻¹ for **TS2-B-1b** and 35.0 kcal·mol⁻¹ for **TS2-B-1c**). Although this tendency does not stand for the resulting intermediates **IM3-B**, it is clear again upon AcOH ligand displacement by CO (−1.2 kcal·mol⁻¹ for **IM4-B-1a**, −2.1 kcal·mol⁻¹ for **IM4-B-1b** and −0.1 kcal·mol⁻¹ for **IM4-B-1c**). It should be emphasized that, in any case, the formation of **IM4-B** is significantly less reversible than the formation of **IM4-A**.

Influence of the solvent. So far, we have analysed the chemoselectivity of the reaction in 1,4-dioxane (ε = 2.25)[9], which is the solvent that was found experimentally to favour the formation of the benzazepinone product. However, at this point, we decided to assess the effect of hexafluoroisopropanol (HFIP) because it was found to be the most effective solvent for promoting carbonylative cyclization of amines via γ-$C(sp^3)$–H activation.[8] Recent studies point toward an important role of this polar acidic solvent in the acceleration of $C(sp^3)$–H cyclopalladation processes, yet its exact role in the reaction remains obscure.[19] Given that HFIP is not available in Gaussian 09, the SMD solvation model for 2-propanol was used in M06 single point energy calculations (hereinafter called HFIP*). Both 2-propanol and HFIP have a similar dielectric constant (ε = 19.9 and 17.8,[20] respectively), although their physical and chemical properties are very different. Consequently, the influence of this change in solvent on the key steps for the two competitive reactions starting from **1a** (formation of **2a** and **3a**) and **1c** (formation of **2c** and **3c**) was analysed comparatively.[21]

As depicted in Table 3, the use of HFIP would make the formation of **IM2-1a** from **IM1-1a** kinetically easier by stabilizing **TS1-1a** [18.1 kcal·mol⁻¹ in 1,4-dioxane and 15.8 kcal·mol⁻¹ when 2-propanol was used as a model for HFIP, (HFIP*)]. However, the change in the solvent has a negligible influence on either the TS energy for the ε-$C(sp^2)$–H bond activation (**TS2-A-1a** is 27.1 kcal·mol⁻¹ in 1,4-dioxane and 26.6 kcal·mol⁻¹ in HFIP*) or the γ-$C(sp^3)$–H cleavage (**TS2-B-1a** is 33.8 kcal·mol⁻¹ in 1,4-dioxane and 33.1 kcal·mol⁻¹ in HFIP*). Nonetheless, both types of C–H activation become less reversible in HFIP because this solvent increases the stability of intermediate **IM4-1a**. However, the $C(sp^3)$–H activation intermediate (**IM4-B-1a**) goes down in energy more pronouncedly (from -1.2 kcal·mol⁻¹ in 1,4-dioxane to -5.2 kcal·mol⁻¹ in HFIP*) than the $C(sp^2)$–H one (**IM4-A-1a**, from 3.8 kcal·mol⁻¹ in 1,4-dioxane to -0.3 kcal·mol⁻¹ in HFIP*), which keeps the latter more reversible than the former.

Table 3. Comparison of the key steps for the competitive synthesis of benzazepinone versus γ-lactam from **1a** and **1c** in 1,4-dioxane and 2-propanol, used as a model for HFIP (*) ($M06_{SMD}$ / 6-311++G(d,p) (C,H,N,O,S,F), SDD (Pd) // B3LYP-D3 / 6-31G(d) (C,H,N,O,S,F), LANL2DZ(f) (Pd)). Relative G values at 298 K (kcal·mol⁻¹).

Ar	Solvent	IM1 dissociation			C–H activation				CO coordination		CO insertion	
		IM1	TS1	IM2	TS2-A	TS2-B	IM3-A	IM3-B	IM4-A	IM4-B	TS3-A	TS3-B
C₆H₅ (**1a**)	1,4-dioxane	0	18.1	13.0	27.1	33.8	17.7	18.8	3.8	-1.2	19.4	22.6
	HFIP*	0	15.8	12.6	26.6	33.1	16.3	18.5	-0.3	-5.2	14.8	15.3
p-CF₃-C₆H₄ (**1c**)	1,4-dioxane	0	20.6	12.7	28.6	35.0	18.9	18.9	4.6	-0.1	21.9	25.3
	HFIP*	0	17.9	10.3	25.7	31.9	16.0	16.3	-2.1	-6.6	15.1	15.1

For subsequent steps, it is interesting to note that both transition states for the CO insertion step (**TS3**) were found to be considerably lower in energy in HFIP*. This stabilization effect is particularly notable for **TS3-B**, related to C(sp³)–H carbonylation (22.6 kcal·mol⁻¹ for **TS3-B-1a** in 1,4-dioxane and 15.3 kcal·mol⁻¹ in HFIP*, compared to 19.4 kcal·mol⁻¹ for **TS3-A-1a** in 1,4-dioxane and 14.8 kcal·mol⁻¹ in HFIP*). As a result, the activation barrier found for the CO insertion leading to benzazepinone **2a** remains almost identical regardless the solvent (15 kcal·mol⁻¹ approximately), whereas it gets significantly reduced for the formation of γ-lactam derivative **3a** (from 23.8 kcal·mol⁻¹ in dioxane to 20.5 kcal·mol⁻¹ in HFIP*).

To sum up, HFIP* as solvent seems to have a profound impact in the reactivity of the system. It clearly favours the formation of **IM2-1a** from **IM1-1a**, through initial ligand displacement of **1a** by AcOH, and it significantly reduces the energy barrier of the CO insertion in the synthesis of γ-lactams derivatives (**3**). Given that the CO insertion was found to be the step with the highest energy barrier for the γ-C(sp³)–H functionalization pathway in 1,4-dioxane, this combined effect could favour a thermodynamic control of the chemoselectivity. Considering electronic effects, this energy barrier lowering effect caused by HFIP becomes more pronounced in the case of substrate **1c**, especially for the CO insertion step leading to the γ-lactam **3c** (25.3 kcal·mol⁻¹ for **TS3-B-1c** in 1,4-dioxane and 15.1 kcal·mol⁻¹ in HFIP).

Experimental studies. In combination with this computational analysis, we conducted a series of experiments to obtain further mechanistic insights in both reaction pathways, the benzazepinone and the γ-lactam synthesis.

Influence of electronic effects on ε-C(sp²)–H bond cleavage. The DFT calculations suggest that the ε-C(sp²)–H functionalization should be favoured in 1,4-dioxane and on increasing the electron-density on the aromatic ring of the substrate. To confirm this premise, we monitored the reaction of γ-phenyl-*allo*-isoleucine derivative **4a**, γ-*p*-tolyl-*allo*-isoleucine derivative **4b**, and γ-*p*-trifluoromethylphenyl-*allo*-isoleucine derivative **4c** using dioxane as the solvent at 110 °C for 2.5 h. Figure 5 shows for each case the reactivity profile from a measure of conversion (%) vs. time (min). The reaction of **4a** required an induction period of 20 min, affording the benzazepinone **5a** in 45% yield. In contrast, the presence of an electron-donating

substituent on the phenyl ring (**4b**) showed enhanced reactivity and no induction time, providing the benzazepinone **5b** in 74% yield under identical conditions. In line with this tendency, the reaction of the electron withdrawing *p*-trifluoromethyl substituent in **4c** hardly reached a 15% conversion after a prolonged induction time of 40 min.

The decreased reactivity and longer induction period observed for **1c** are in complete agreement with the theoretical calculations, which predicted a higher activation barrier to reach **TS1** from dissociation of **IM1-1c** to generate the active complex **IM2-1c** (see Table 2). At this point, we reasoned that given that the formation of the active **IM2** intermediate presumably takes place by displacement of one unit of **1a** by AcOH (see Figure 1), the addition of AcOH might have a beneficial effect in the acceleration of this ligand exchange, thereby increasing the reactivity. To test this hypothesis, the carbonylative cyclization of **4a** was performed in the presence of AcOH as additive (6.0 equiv). As shown in Figure 5, this small modification led to a suppression of the induction period and did indeed result in a significant rate enhancement, enabling the formation of the corresponding product with higher conversion (red line).
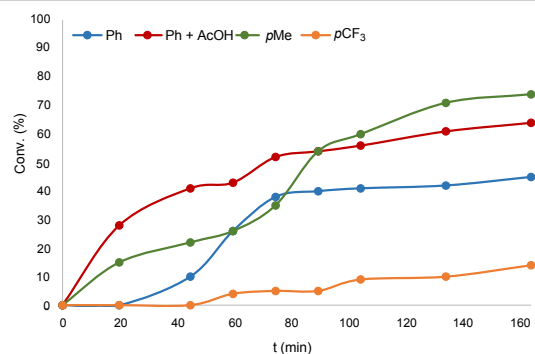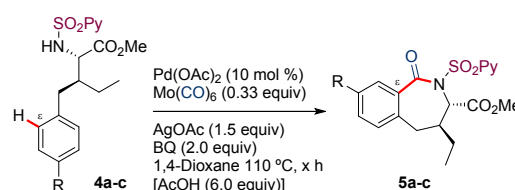
Figure 5. Reactivity profile [conversion (%) *vs* time (min)] of **4a**, **4b** and **4c**. Conversions determined by ^{1}H NMR.

Deuterium labelling experiments. In addition to affecting reactivity, the electronic effects also have a profound impact in selectivity. Theoretical calculations supported our previous findings that substrates with electron-rich aromatic substituents showed strong preference for the C(sp^2)–H activation pathway, whereas ones with electron neutral or electron withdrawing demand displayed lower selectivity. This loss of selectivity can be attributed to an enhancement of the reversibility of the ε-C(sp^2)–H activation process (see Table 2). To confirm this statement, we next conducted intermolecular deuterium-labelling competition experiments in parallel using **4a**, **4b** and **4c** (Scheme 2) as starting materials. The reactions were carried out in the presence of d$_4$-acetic acid (6.0 equiv), under otherwise standard conditions, and stopped at a low conversion (4 h). The carbonylation reaction of **4a** resulted in deuterium incorporation at the *ortho*-position of both, the product (**5a-D**, 44% yield, 33% D) and the recovered starting material **4a-D** (56% yield, 62% D). For substrate **4b**, less significant deuterium/hydrogen scrambling was observed in both, the product (**5b-D**, 38% yield, 17% D) and the starting material (**4b-D**, 62% yield, 54% D). In contrast, incorporation of deuterium was significantly increased in the case of **4c**, bearing a CF$_3$ group in the aryl ring. In this case, a 35% of deuterium incorporation in the product (**5c-D**, 25% yield) and 71% H/D scrambling for the starting material (**4c-D**, 75% yield) was observed.

These deuterium labelling experiments are consistent with computational modelling and reveal that the C(sp^2)–H activation is a reversible process and that the reverse reaction seems to become faster with more electron-deficient aromatic systems.
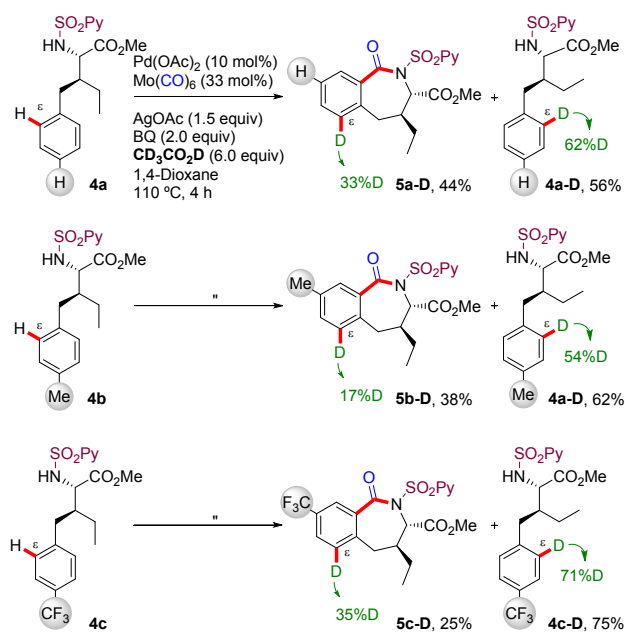
Scheme 2. Deuterium-labelling experiments from substrates **4a**, **4b** and **4c**.

Next, to check whether the reversibility of the ε-C(sp^2)–H bond cleavage might be affected by the competing γ-C(sp^3)–H bond functionalization, the model substrate **1a** was subjected to the same deuterium-labelling experiment (Scheme 3). The carbonylation reaction of **1a** resulted in D-incorporation at the *ortho*-position of either the benzazepinone product **2a-D** (31% yield, 17% D) or the γ-lactam **3a-D** (33% yield, 21% D), as well as the recovered starting material **1a-D** (34% yield, 49% D). In any case, the D/H scrambling at the ε position was lower than that observed in the experiment with **4a**. These results suggest that the ε-C(sp^2)–H bond cleavage is reversible and it competes with the γ-C–H bond activation process that leads to the formation of the γ-lactam.
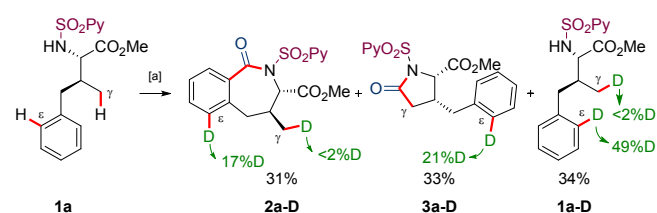
Scheme 3. [a] Reaction conditions: **1a** (0.10 mmol), Mo(CO)$_6$ (0.033 mmol, 30 mol %), Pd(OAc)$_2$ (0.01 mmol, 10 mol %), AgOAc (0.15 mmol, 1.5 equiv), 1,4-benzoquinone (BQ) (0.20 mmol, 2.0 equiv), CD$_3$CO$_2$D (6.0 equiv), 1,4-dioxane (0.40 mL) 110 °C, 4 h, under argon atmosphere.

Studies towards reversal of chemoselectivity. The combined studies suggest that the key feature that enables switching the chemoselectivity towards the synthesis of the γ-lactam relies on tunning the reversibility of the ε-C(sp^2)–H bond cleavage to favour the thermodynamic control of the process. To gain an understanding on the factors influencing this process, we carried out a systematic study of the main parameters that control the reactivity of the key catalytic intermediate species: i) amount/source of carbon monoxide; ii) the use of AcOH as additive; and iii) the solvent effect.
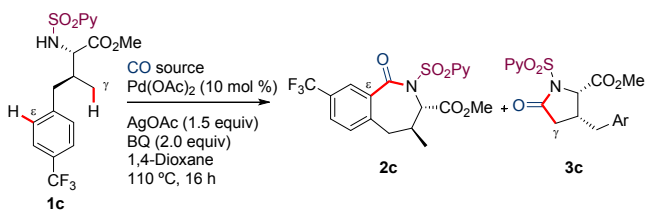
Influence of the amount/source of CO. According to the DFT calculations, the coordination of CO to the C(sp^3)–H cyclopalladated intermediate by displacement of AcOH makes irreversible the formation of the resulting intermediate **IM4-B**, in contrast to the pathway leading to the analogue ε-C(sp^2)–palladacyle **IM4-A**, which remained reversible (Figure 2). Consequently, the concentration of CO generated from Mo(CO)$_6$, could play an important role in controlling reactivity and chemoselectivity. The influence of this reaction parameter was evaluated by performing the reaction of the less reactive compound **1c** under variable amounts of Mo(CO)$_6$ (Table 4). An attenuation of the catalytic activity towards the synthesis of the γ-lactam **3c** was observed by increasing the amount of Mo(CO)$_6$ from 33 mol% to 83 mol%, while this change marginally affected the formation of benzazepinone **2c** (compare entries 1 and 3). However, lowering the amount of Mo(CO)$_6$ resulted in an increased formation of γ-lactam **3c** without affecting the formation of **2c** (entry 2). This effect is in accordance with the theoretical calculations that suggest a less reversible character of the C(sp^2)–H activation process at higher concentrations of CO, thus favouring the kinetically preferred benzazepinone product. On the other hand, when the reaction of **1c** was carried

out under gaseous CO (1 atm, sealed tube), the starting material was recovered unaltered (entry 3). This lack of reactivity might be due to either the reducing ability of CO that could induce the reduction of Pd(II) species to Pd(0), or the inhibition of the C–H activation event by competitively occupying coordination sites in the Pd(II) center.[22]

Effect of using AcOH as additive. The DFT studies point toward an important role of AcOH in promoting an endergonic ligand displacement from **IM1** to reach the active intermediate **IM2** (Figure 1). Additionally, AcOH/CO ligand exchange is required prior to the CO insertion step (from **IM3** to **IM4**, Figure 2). However, although formation of **IM4** is an exergonic step in both C(sp^2)–H and C(sp^3)–H activation pathways, the lower energy gap between **IM3-A** and **IM4-A** (for the ε-C(sp^2)–palladacyle) makes this process reversible, whereas formation of the γ-C(sp^3)–palladacyle **IM4-A** is much more exergonic and seems to be irreversible. Therefore, the addition of AcOH might provide, not only cause an increase in catalytic activity (by reducing the induction period), but also a high reversibility of the ε-C(sp^2)–H bond cleavage (by accelerating the reverse **IM4-A→IM3-A** process), thereby favoring the thermodynamic control of the reaction towards γ-lactam formation.

As shown in Table 4, the addition of AcOH (3.0 equiv) to the carbonylative cyclization of **1c** favourably impacted the selectivity towards the formation of γ-lactam **3c** (37% isolated yield, along with 18% of benzazepinone **2c**, entry 5). To our delight, when this effect was combined with the use of hexafluoroisopropanol as solvent and adjustment of the concentration to 0.125 M, the yield of the γ-lactam **3c** raised up to 63% while no benzazepinone was detected by ^{1}H NMR of the crude mixture (entry 6). A control experiment confirmed that, although the presence of AcOH slightly decreased the conversion (likely by inhibiting its ligand exchange with CO), it was key for attaining complete selectivity towards the γ-lactam (entry 7). Both, the effect of AcOH and HFIP operate in gratifying agreement with prior computational studies.

**Table 4.** Optimization studies towards γ-lactam derivative **3c**.

Entry[a]	CO source	Solvent (conc.)	Additive	2c (%)[b]	3c (%)[b]
1	Mo(CO)$_6$ (33 mol%)	1,4-dioxane (0.25 M)	–	22	21
2	Mo(CO)$_6$ (17 mol%)	1,4-dioxane (0.25 M)		21	28
3	Mo(CO)$_6$ (83 mol%)	1,4-dioxane (0.25 M)		23	15
4	CO (g) (1 atm)	1,4-dioxane (0.25 M)		–	–
5	Mo(CO)$_6$ (33 mol%)	1,4-dioxane (0.25 M)	AcOH	18	37
6	Mo(CO)$_6$ (33 mol%)	HFIP (0.125 M)	AcOH	–	63
7	Mo(CO)$_6$ (33 mol%)	HFIP (0.125 M)	–	10	69

[a] Reaction conditions: **1c** (0.10 mmol), CO source, Pd(OAc)$_2$ (0.01 mmol, 10 mol %), AgOAc (0.15 mmol, 1.5 equiv), 1,4-benzoquinone (BQ) (0.20 mmol, 2.0 equiv), solvent, additive (3.0 equiv), 110 °C, 16 h, under argon atmosphere. [b] Isolated yields.

Scope and application to late-stage diversification. The synthetic utility of the new protocol for the γ-C(sp^3)–H bond functionalization was shown by utilizing diverse γ-arylated L-valine derivatives (Scheme 4). Regardless the substitution pattern (*para*, *meta*, *ortho*), the presence of an electron-withdrawing group on the phenyl ring ensures the obtention of the corresponding γ-lactam derivatives in good yields and selectivities (γ/ε from 6.9:1 to >20:1). Important from a further elaboration standpoint, the system tolerates halogens (Cl, Br, F), ester and nitro groups. Interestingly, the γ-lactam product was formed preferentially over the benzazepinone product even when electron-rich aryl-substituted substrates were tested (products **3b**, **3d**, **3j** and **3l**), albeit with lower selectivity (γ/ε from 1.2:1 to 4.7:1). As a reminder, the γ-lactam product was not even detected in the reaction mixture of the carbonylative cyclization of this type of substrates under our prevously developed method.[9]

Finally, the seemingly relevant stabilization role of the ester group (through its carbonyl moiety) of the α-amino acid moiety predicted by the theoretical calculations compelled us to examine the simple amine **6b**, analogous to **3b** but lacking the α-ester moiety (Scheme 5). Despite the electron-rich nature of the aromatic ring in **6b**, the corresponding γ-lactam was the only product observed in the carbonylation/cyclization reaction, although the yield was modest (30%) due to a low conversion. In this case, the difference in energy between **TS2-A** and **TS2-B**, calculated in 1,4-dioxane, is only 4.0 kcal·mol^{-1} (compare with the difference of 6.4 kcal·mol^{-1} calculated for **1b**, as shown in Table 2), probably due to the lack of stabilizing interaction between the carbonyl oxygen of the ester group and

the Pd center. Therefore, the kinetic preference of this substrate for the ε-C(sp^2)–H is lower than in the case of α-amino acid derivatives, thus favoring γ-C(sp^3)–H selectivity.
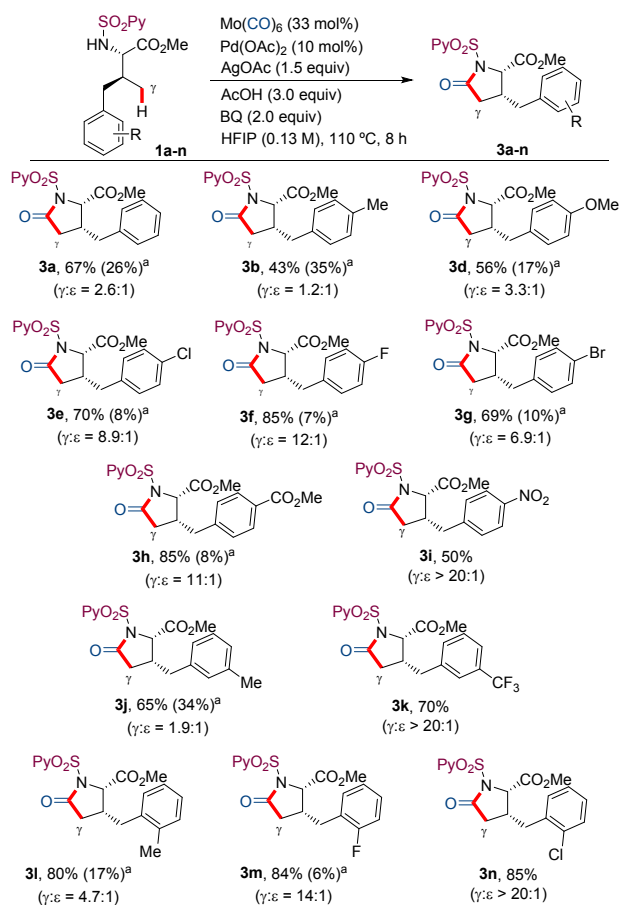

Scheme 4. Scope of the *N*-SO$_2$Py-assisted Pd-catalyzed carbonylative cyclization reaction at γ-C(sp^3)–H bonds. Isolated yields after column chromatography. ^{a} In parenthesis, isolated yield of C(sp^2)–H activation product.
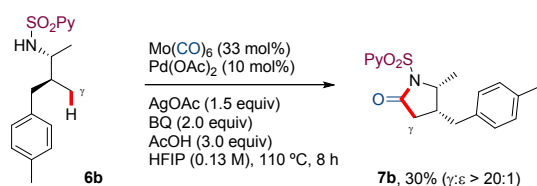
Scheme 5. Scope of the *N*-SO$_2$Py-assisted Pd-catalyzed carbonylative cyclization reaction at γ-C(sp^3)–H bonds.

The increased complexity of small peptides represents a demanding test for the late-stage functionalization capability of this method.[23] We were delighted to find that the reaction of dipeptide derivative **8** took place with high chemoselectivity, albeit with low conversion, providing the corresponding modified peptide **9** in a meritorious 32% yield (Scheme 6).
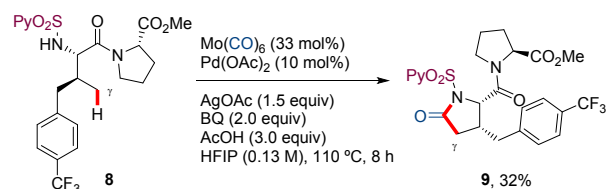
Scheme 6. Carbonylative cyclization of dipeptide **8**.

Conclusions

In conclusion, the combination of experimental and computational studies has allowed to gain a solid understanding on the factors that control chemoselectivity in competing ε-C(sp^2)–H and γ-C(sp^3)–H activation pathways in the palladium-catalyzed carbonylative cyclization of γ-arylated valine derivatives. Taken together, all this knowledge has provided the basis for the rational identification of reaction conditions that enable reversing the conventional selectivity for arene C(sp^2)–H activation displayed by Pd, providing the access to γ-lactam derivatives through C(sp^3)–H cleavage. The success of this development hinges upon the faster and reversible character of the ε-C(sp^2)-H activation compared to the γ-C(sp^3)–H activation, along with the higher thermodynamic stability of the subsequent palladacycle intermediates formed upon AcOH/CO exchange and CO insertion in the latter case. The use of AcOH as additive and HFIP as solvent were found to play a key role for favoring thermodynamic control by acceleration of the reversible C(sp^2)–H activation pathway while slowing down the AcOH/CO exchange.

Conflicts of interest

There are no conflicts to declare.

Acknowledgements

References

1   For selected general reviews on C–H functionalization: (a) X. Chen, K. M. Engle, D.-H. Wang and J.-Q. Yu, *Angew. Chem., Int. Ed.*, 2009, **48**, 5094–5115; (b) T. W. Lyons and M. S. Sanford, *Chem. Rev.*, 2010, **110**, 1147–1169; (c) O. Daugulis, J. Roane and L. D. Tran, *Acc. Chem. Res.*, 2015, **48**, 1053–1064; (d) T. Gensch, M. N. Hopkinson, F. Glorius and J. Wencel-Delord, *Chem. Soc. Rev.*, 2016, **45**, 2900–2906; (e) J. F. Hartwig, *J. Am. Chem. Soc.*, 2016, **138**, 2–24; (f) J. F. Hartwig and M. A. Larsen, *ACS Cent. Sci.*, 2016, **2**, 281–292; (g) P. Gandeepan, T. Muller, D. Zell, G. Cera, S. Warratz and L. Ackermann, *Chem. Rev.*, 2019, **119**, 2192–2452.

2   For reviews on late-stage C–H diversification: (a) D. Y.-K. Chen and S. W. Youn, *Chem. Eur. J.*, 2012, **18**, 9452–9474; (b) T. Cernak, K. D. Dykstra, S. Tyagarajan, P. Vachal and S. W. Krska, *Chem. Soc. Rev.*, 2016, **45**, 546–576; (c) S. Sengupta and G. Mehta, *Tetrahedron Lett.*, 2017, **58**, 1357–1372; (d) W. Wang, M. M. Lorion, J. Shah, A. R. Kapdi and L. Ackermann, *Angew. Chem. Int. Ed.*, 2018, **57**, 14700–14717; (e) R. R. Karimov and J. F. Hartwig, *Angew. Chem. Int. Ed.*, 2018, **57**, 4234–4241; (f) X. Lu, S-J. He, W.-M. Cheng and J. Shi, *Chin. Chem. Lett.*, 2018, **29**, 1001–1008.

3   For reviews on the use of directing groups in C–H functionalization: (a) S. R. Neufeldt and M. S. Sanford, *Acc. Chem. Res.*, 2012, **53**, 9426–9428; (b) G. Rouquet and N. Chatani, *Angew. Chem. Int. Ed.*, 2013, **52**, 11726 –11743; (c) M. Zhang, Y. Zhang, X. Jie, H. Zhao, G. Li and W. Su, *Org. Chem. Front.*, 2014, **1**, 843–895; (d) Q. Zhao, T. Poisson, X. Pannecoucke and T. Besset, *Synthesis*, 2017, **49**, 4808–4826; (e) P. Gandeepan and L. Ackermann, *Chem*, 2018, **4**, 199–222; (f) O. K. Rasheed and B. Sun, *ChemistrySelect*, 2018, **3**, 5689–5708; (g) C. Sambiagio, D. Schönbauer , R. Blieck, T. Dao-Huy, G. Pototschnig, P. Schaaf, T. Wiesinger, M. F. Zia, J. Wencel-Delord, T. Besset, B. U. W. Maes and M Schnürch, *Chem. Soc. Rev.,* 2018, **47**, 6603–6743 (h) B. Niu, K. Yang, B. Lawrence and H. Ge, *ChemSusChem*, 2019, **12**, 2955–2969; (i) S. St John-Campbell and J. A. Bull, *Org. Biomol. Chem.*, 2018, **16**, 4582–4595; (j) S. Rej, Y. Ano and N. Chatani, *Chem. Rev.*, 2020, **120**, 1788–1887.

4   For a general review on metal-catalyzed regiodivergent reactions: (a) C. Nájera, I. P. Beletskaya and M. Yus, *Chem. Soc. Rev.,* 2019, **48**, 4515–4618. For selected examples, see: (b) B. S. Lane, M. A. Brown and D. Sames, *J. Am. Chem. Soc.*, 2005, **127**, 8050–8057; (c) N. P. Grimster, C. Gauntlett, C. R. A. Godfrey and M. J. Gaunt, *Angew. Chem., Int. Ed.*, 2005, **44**, 3125–3129; (d) E. M. Beck, N. P. Grimster, R. Hatley and M. J. Gaunt, *J. Am. Chem. Soc.*, 2006, **128**, 2528–2529; (e) R. J. Phipps and M. J. Gaunt, *Science*, 2009, **323**, 1593–1597; (f) D. J. Schipper, L.-C. Campeau and K. Fagnou, *Tetrahedron*, 2009, **65**, 3155–3164; (g) K. Ueda, S. Yanagisawa, J. Yamaguchi and K. Itami, *Angew. Chem., Int. Ed.*, 2010, **49**, 8946–8949; (h) D. Lapointe, T. Markiewicz, C. J. Whipp, A. Toderian and K. Fagnou, *J. Org. Chem.*, 2011, **76**, 749–759; (i) X. Zhang, W. Si, M. Bao, N. Asao, Y. Yamamoto and T. Jin, *Org. Lett.*, 2014, **16**, 4830–4833; (j) J. D. Dooley, S. R. Chidipudi and H. W. Lam, *J. Am. Chem. Soc.*, 2013, **135**, 10829–10836; (k) A. M. Wagner, A. J. Hickman and M. S. Sanford, *J. Am. Chem. Soc.*, 2013, **135**, 15710–15713; (l) H.-X. Dai, G. Li, X.-G. Zhang, A. F. Stepan and J.-Q. Li, *J. Am. Chem. Soc.*, 2013, **135**, 7567–7571; (m) W. B. Cross, S. Razak, K. Singh and A. J. Warner, *Chem.–Eur. J.*, 2014, **20**, 13203–13209; (n) X. Cong and X. Zheng, *Org. Lett.*, 2014, **16**, 3716–3719; (o) M.-S. Yu, W.-C. Lee, C.-H. Chen, F.-Y. Tsai and T.-G. Ong, *Org. Lett.*, 2014, **16**, 4826–4828; (p) W. Du, Q. Gu, Z. Li and D. Yang, *J. Am. Chem. Soc.*, 2015, **137**, 1130–1135; (q) R. B. Bedford, S. J. Durrant and M. Montgomery, *Angew. Chem. Int. Ed.*, 2015, **54**, 8787–8790; (r) D. Kang and S. Hong, *Org. Lett.*, 2015, **17**, 1938–1941; (s) S. R. Neufeldt, G. Jiménez-Osés, J. R. Huckins, O. R. Thiel and K. N. Houk, *J. Am. Chem. Soc.*, 2015, **137**, 9843–9854; (t) R. Santhoshkumar, S. Mannathan and C.-H. Cheng, *J. Am. Chem. Soc.*, 2015, **137**, 16116–16120; (u) S. Li, H. Ji, L. Cai and G. Li, *Chem. Sci.*, 2015, **6**, 5595–5600; (v) Y. Su, S. Gao, Y. Huang, A. Lin and H. Yao, *Chem.– Eur. J.*, 2015, **21**, 15820–15825; (w) I. Sasaki, J. Taguchi, S. Hiraki, H. Ito and T. Ishiyama, *Chem.– Eur. J.*, 2015, **21**, 9236–9241; (x) S. Lee, S. Mah and S. Hong, *Org. Lett.*, 2015, **17**, 3864–3867; (y) A. M. Martínez, J. Echavarren, I. Alonso, N. Rodríguez, R. Gómez Arrayás and J. C. Carretero, *Chem. Sci.*, 2015, **6**, 5802-5814; (z) Y.-H. Sun, T.-Y. Sun, Y.-D. Wu, X. Zhang and Y. Rao, *Chem. Sci.*, 2016, **7**, 2229–2238; (aa) Y. Li, F. Xie and X. Li, *J. Org. Chem.*, 2016, **81**, 715–722; (ab) A. C. Shaikh, D. R. Shinde and N. T. Patil, *Org. Lett.*, 2016, **18**, 1056–1059; (ac) H. T. Kim, H. Ha, G. Kang, O. S. Kim, H. Ryu, A. K. Biswas, S. M. Lim, M.-H. Baik and J. M. Joo, *Angew. Chem., Int. Ed.*, 2017, **56**, 16262–16266; (ad) S. Okumura, T. Tomine, E. Shigeki, K. Semba and Y. Nakao, *Angew. Chem., Int. Ed.*, 2018, **57**, 929–932; (ae) D.-W. Yin and G. Liu, *J. Org. Chem.*, 2018, **83**, 3987–4001.

5   (a) L.-C. Campeau, D. J. Chipper and K. Fagnou, *J. Am. Chem. Soc.*, 2008, **130**, 3266–3267; (b) D. J. Schipper, L.-C. Campeau and K. Fagnou, *Tetrahedron*, 2009, **65**, 3155–3164; (c) P. Novák, A. Correa, J. Gallardo-Donaira and R. Martin, *Angew. Chem., Int. Ed.*, 2011, **50**, 12236–12239; (d) F.-L. Zhang, K. Hong, T.-J. Li, H. Park and J.-Q. Yu, *Science*, 2016, **351**, 252–256; (e) F. Ma, M. Lei and L. Hu *Org. Lett.*, 2016, **18**, 2708–2711; (f) H. Park, K. Yoo, B. Jung and M. Kim, *Tetrahedron*, 2018, **74**, 2048–2055; (g) Q. He, Y. Ano and N. Chatani, *Chem. Commun.,* 2019, **55**, 9983–9986; (h) H. Park, P. Verma, K. Hong and J.-Q. Yu, *Nat. Chem.*, 2018, **10**, 755–762; (i) G. Hong, P. D. Nahide, U. K. Neelam, P. Amadeo, A. Vijeta, J. M. Curto, C. E. Hendrick, K. F. VanGelder and M. C. Kozlowski, *ACS Catal.*, 2019, **9**, 3716–3724. Just before submitting this manuscript, the only example existing in the literature describing a chemodivergent procedure targeting either C(sp^3)–H or C(sp^2)–H bond activation at a single substrate has appeared, which uses temperature as the element for chemoselectivity control: T. Gogula, J.n Zhang, M. R. Lonka, S. Zhang and H. Zou, *Chem. Sci.-Accepted Manuscript*, DOI: 10.1039/D0SC02328K.

6   For regiodivergent functionalization at two C(sp^3)–H bonds: D. Katayev, E. Larionov, M Nakanishi, C. Besnard and E. P. Kundig, *Chem.– Eur. J.*, 2014, **20**, 15021–15030.

7   For reviews, see: (a) A. F. M. Noisier and M. A. Brimble, *Chem. Rev.*, 2014, **114**, 8775–8806; (b) G. He, B. Wang, W. A. Nack and G. Chen, *Acc. Chem. Res.*, 2016, **49**, 635–645; (c) X. Lu, B. Xiao, R.; Shang and L. Liu, *Chin. Chem. Lett.*, 2016, **27**, 305–311; (d) M. Zhang, Q. Wang, Y. Peng, Z. Chen, C. Wan, J. Chen, Y. Zhao, R. Zhang and A. Q. Zhang, *Chem. Commun.*, 2019, **55**, 13048–13065; (e) A. Trowbridge, S. M. Walton and M. J. Gaunt, *Chem. Rev.*, 2020, **120**, 2613–2692. For a general review on C(sp^3)-H activation: (f) J. He, M. Wasa, K. S. L. Chan, Q. Shao and J.-Q. Yu, *Chem. Rev.*, 2017, **117**, 8754–8786.

8   E. Hernando, J. Villalva, A. M. Martinez, I. Alonso, N. Rodríguez, R. G. Arrayás and J. C. Carretero, *ACS Catal.*, 2016, **6**, 6868–6882.

9   M. Martínez-Mingo, N. Rodríguez, R. Gómez Arrayás and J. C. Carretero, *Org. Lett.*, 2019, **21**, 4345–4349.

10   (a) B.-J. Li, S.-L. Tian, Z. Fang and Z.-J. Shi, *Angew. Chem., Int. Ed.*, 2008, **47**, 1115–1118; (b) D. Balcells, E. Clot and O. Eisenstein, *Chem. Rev.*, 2010, **110**, 749–823; (c) C. Wang, C. Chen, J. Zhang, J. Han, Q. Wang, K. Guo, P. Liu, M. Guan, Y. Yao and Y. Zhao, *Angew. Chem. Int. Ed.*, 2014, **53**, 9884–9888; (d) H. Lin, X. Pan, A. L. Barsamian, T. M. Kamenecka and T. D. Bannister, *ACS Catal.*, 2019, **9**, 4887–4891.

11   Trinuclear [Pd$_3$(OAc)$_6$] was optimized on the basis of the single crystal structure reported in the following reference: A. C. Skapski and M. L. Smart, *J. Chem. Soc. D*, 1970, 658b-659.

12   Athough the generation of alloyed-metal nanoparticles that could be catalytically competent cannot be ruled out, we found reasonable to assume that the metal-containing species are involved homogeneously on the basis of two observations. The first one is that most of the precedents related to palladium catalyzed carbonylative transformations mediated by Mo(CO)$_6$ have been proposed to occur under a homogenous catalysis regime, even in the presence of superstoichiometric amounts of silver salts (for a review, see: (a) L. Åkerbladh, L. R. Odell and M. Larhed, Synlett, 2019, *30*, 141–155; see also: Z. Wang, Y. Li, F. Zhu and X.-F. Wu, *Adv. Synth. Catal.*, 2016, **358**, 2855–2859). The second reason is that we have observed mononuclear palladium complexes

upon high resolution ESI-MS monitoring of the carbonylative cyclization of substrate **4a** using a preformed palladium-complex of **4a** (10 mol%) as precatalyst under otherwise identical optimized reaction conditions (see ref. 9).

13 (a) W. Liu, J. Zheng, Z. Liu, W. Hu, X. Wang and Y. Dang, *ACS Catal.*, 2018, **8**, 7698–7709; (b) B. E. Haines, J. F. Berry, J.-Q. Yu and D. G. Musaev, *ACS Catal.*, 2016, **6**, 829-839; (c) V. I. Bakhmutov, J. F. Berry, F. A. Cotton, S. Ibragimovb and C. A. Murillo, *Dalton Trans.*, 2005, 1989–1992; (d) W. Feng, T. Wang, D. Liu, X. Wang and Y. Dang, *ACS Catal.*, 2019, **9**, 6672–6680.

14 The reaction of equimolecular amounts of the γ-arylated *allo*-isoleucine *N*-SO$_2$Py derivative with Pd(OAc)$_2$ in 1,4-dioxane under argon atmosphere at 110 °C for 1 h leads to the formation of a Pd^{II}-complex with two units of γ-arylated *allo*-isoleucine *N*-SO$_2$Py derivative coordinated to the Pd atom as mono-anionic bidentate *N,N*-donor ligands. The single crystal structure of this complex was reported in reference 9.

15 A reaction pathway including the trinuclear species Pd$_3$(OAc)$_6$ cannot be ruled out: J. Váňa, J. Lang, M. Šoltésová, J. Hanusek, A. Růžička, M. Sedláka and J. Roithová, *Dalton Trans.*, 2017, **46**, 16269–16275.

16 Since in the stoichiometric reaction the formation of complex **IM1-1a** and its reaction with Mo(CO)$_6$ take place without AgOAc, providing cleanly the carbonylation product **2a**, we might intuitively rule out that the Ag salt is necessary for the C–H activation step to take place (see SI for details). Instead, the Ag salt is likely acting as an oxidant for the palladium center. However, silver salts could also be involved in the formation of hetero-bimetallic Pd-Ag species, which could participate in the C–H activation step. See: (a) Y.-F. Yang, G.-J. Cheng, P. Liu, D. Leow, T.-Y. Sum, P. Chen, X. Zhang, Y.-Q. Yu, Y.-D. Wu and K. N. Houk, *J. Am. Chem. Soc.*, 2014, **136**, 344–355; (b) M. Anand, R. B. Sunoj and H. F. III Schaefer, *J. Am. Chem. Soc.*, 2014, **136**, 5535–5538; (c) M. Anand, R. B. Sunoj and H. F. III Schaefer, *ACS Catal.*, 2016, **6**, 696-708. We have also tried to shed light on this point by calculating the possible heterobimetallic Pd-Ag intermediates and transition states that could be involved in our C–H activation process but we could not find any more favourable pathway either from **IM1-1a** or **IM2-1a** (see SI for details). For a recent investigation of the role of silver carboxylate salts in Pd-catalyzed arene C–H functionalization, see: (d) M. D. Lotz, N. M. Camasso, A. J. Canty and M. S. Sanford, *Organometallics*, 2016, **36**, 165–171; (e) Y. Shimoyama, J. Kuwabara and T. Kanbara, *ACS Catalysis*, 2020, **10**, 3390–3397 (and references therein).

17 J-J. Li, R. Giri and J-Q. Yu, *Tetrahedron*, 2008, **64**, 6979-6987.

18 Previous calculations by our group had revealed the convenience of coordinating an additional CO unit to reach a favorable transition state for the CO migratory insertion step. See reference 8. The extraordinary stability of CO-coordinated palladacycles seems to be at the origin of its reluctance for migratory insertion (see: Y. Jiang, S-Q. Zhang, F. Cao, J.-X. Zou, J-L. Yu, B-F. Shi, X. Hong and Z. Wang, *Organometallics*, 2019, **38**, 2022–2030). In the current study, the CO migratory insertion steps from complexes carrying only one unit of CO, as well as assisted by AgOAc, have also been evaluated giving rise to much higher barriers (see SI for details).

19 C. Yu, J. Sanjosé-Orduna, F. W. Patureau and M. H. Pérez-Temprano, *Chem. Soc. Rev.*, 2020, **49**, 1643–1652.

20 (a) M. Fioroni, K. Burger, A. E. Mark and D. Roccatano, *J. Phys. Chem. B*, 2001, **105**, 10967-10975; (b) D. Hong, M. Hoshino, R. Kuboi and Y. Goto, *J. Am. Chem. Soc.*, 1999, **121**, 8427–8433.

21 This analysis has also been done using **1b**, giving rise to a slight variation in the stability of key intermediates that become lower than for **1a** (see SI for details). In the case of **TS1** and **TS3**, that seem to be more sensitive to solvent effects, structures were reoptimized including solvent in the optimization process. Data resulted comparable to those collected in table 3, although HFIP provoked a lower stabilization of **TS1** but a higher of **TS3** (see SI for details).

22 According to our previous calculations (see ref 8), the transition state for the C–H activation would be less stable since CO coordinates Pd center displacing pyridine ligand.

23 For a recent review on late-stage peptide diversification by C–H activation, see ref 2d.